Title

Hybrid Mouse Diversity Panel Identifies Genetic Architecture Associated with the Acute Antisense Oligonucleotide-Mediated Inflammatory Response to a 2-O-Methoxyethyl Antisense Oligonucleotide.

Journal

Nucleic Acid Therapeutics, 29(5)

Authors

Pirie, Elaine
Cauntay, Patrick
Fu, Wuxia
et al.

Publication Date

2019-10-01

DOI

10.1089/nat.2019.0797

Peer reviewed

NUCLEIC ACID THERAPEUTICS
Volume 29, Number 5, 2019

DOI: 10.1089/nat.2019.0797

Hybrid Mouse Diversity Panel Identifies Genetic Architecture Associated with the Acute Antisense Oligonucleotide-Mediated Inflammatory Response to a 2′-*O*-Methoxyethyl Antisense Oligonucleotide

Elaine Pirie,[1] Patrick Cauntay,[2] Wuxia Fu,[1] Shayoni Ray,[1,*] Calvin Pan,[3] Aldonis J. Lusis,[3] Jill Hsiao,[2] Sebastien A. Burel,[2] Padma Narayanan,[2] Rosanne M. Crooke,[1] and Richard G. Lee[1]

Although antisense oligonucleotides (ASOs) are well tolerated preclinically and in the clinic, some sequences of ASOs can trigger an inflammatory response leading to B cell and macrophage activation in rodents. This prompted our investigation into the contribution of genetic architecture to the ASO-mediated inflammatory response. Genome-wide association (GWA) and transcriptomic analysis in a hybrid mouse diversity panel (HMDP) were used to identify and validate novel genes involved in the acute and delayed inflammatory response to a single 75 mg/kg dose of an inflammatory 2′-*O*-methoxyethyl (2′MOE) modified ASO. The acute response was measured 6 h after ASO administration, via evaluation for increased plasma production of interleukin 6 (IL6), IL10, monocyte chemoattractant protein 1 (MCP-1) and macrophage inflammatory protein-1β (MIP-1β). Delayed inflammation was evaluated by spleen weight increases after 96 h. We identified single nucleotide polymorphisms (SNPs) on chromosomes 16 and 17 associated with plasma MIP-1β, IL6, and MCP-1 levels, and one on chromosome 8 associated with increases in spleen weight. Systems genetic analysis utilizing transcriptomic data from HMDP strain macrophages determined that the acute inflammatory SNPs were expression quantitative trait locis (eQTLs) for CCAAT/enhancer-binding protein beta (*Cebpb*) and salt inducible kinase 1 (*Sik1*). The delayed inflammatory SNP was an eQTL for Rho guanine nucleotide exchange factor 10 (*Arhgef10*). *In vitro* assays in mouse primary cells and human cell lines have confirmed the HMDP finding that lower *Sik1* expression increases the acute inflammatory response. Our results demonstrate the utility of using mouse GWA study (GWAS) and the HMDP for detecting genes modulating the inflammatory response to pro-inflammatory ASOs in a pharmacological setting.

Keywords: inflammation, GWAS, oligonucleotide, eQTL

Introduction

Antisense oligonucleotides (ASOs) are a well-recognized, potent therapeutic platform used in the clinic to treat a variety of human conditions, including cardiometabolic, infectious, inflammatory, and neurological disease [1–7]. By utilizing short synthetic (12–24mer) chemically modified DNA-like oligonucleotides to bind complimentary mRNA sequences, ASOs are able to modulate the degradation, splicing, and regulation of mRNA in a highly selective, sequence-specific manner [8]. In the most commonly applied mechanism, an ASO binds complementary mRNA and induces RNAseH1-mediated degradation, preventing translation and thus reducing the overall quantity of the target protein [9]. Iterative platform modifications throughout the past 30 years have increased stability, potency, specificity, and reduced toxicity. In particular, the modification of the phosphodiester backbone to 2′-*O*-methoxyethyl (2′MOE) has not only significantly increased stability and potency but also reduced ASO-mediated inflammation [10–15].

The past several decades have seen rapid expansion in our understanding of the cell surface and endosome-associated toll-like receptors (TLRs), of which TLR 3, 7, 8, and 9 recognize

[1]Cardiovascular Antisense Drug Discovery Group, Ionis Pharmaceuticals, Carlsbad, California.
[2]Preclinical Development, Ionis Pharmaceuticals, Carlsbad, California.
[3]Department of Human Genetics, University of California, Los Angeles, Los Angeles, California.
*Current affiliation: Space Biosciences Division, USRA/NASA Ames Research Center, Moffett Field, California.

nucleic acids [16–19]. Early structure–activity relationship studies determined that unmethylated cytosine-guanine (CpG) motifs, common in bacteria and DNA viruses, have reduced frequency and increased methylation in vertebrates, thus acting as a ligand for TLR9 [20,21]. Activation of TLR9 in the endosome signals via myeloid differentiation of primary response genes 88 (*Myd88*), triggering the activation of mitogen-activated protein kinase (*MAPK*) family members and nuclear factor kappa-light-chain-enhances of activated B cells (*NF-κB*) signaling pathways [19,21,22]. In addition, receptor for advance glycation end product (*RAGE*) has been shown to promote inflammatory responses on interaction with CpG-containing ligands at the cell surface, provoking endosomal uptake and further contact with TLR9, leading to enhanced *NF-κB* signaling [23].

Previous work has demonstrated that non-CpG containing 2′MOE ASOs are able to activate splenic B cells and macrophage populations, and this response is dependent on MyD88 and TLR9 function [24]. Further, the RAGE receptor is involved in mediating the inflammatory response to systemic administration of non-CpG containing sequences [23]. Aside from TLR9-mediated stimulation, ASOs are able to initiate TLR9 and Myd88 independent proinflammatory responses as well [15,25].

Therefore, although ASOs are widely accepted, effective therapeutic agents and are generally well tolerated in the clinic, a small number of sequences are capable of triggering an inflammatory response, resulting in B cell and macrophage activation in rodents *in vivo* [15,24]. These sequences are not utilized as clinical candidates. However, an understanding of the mechanism of the proinflammatory effects of these sequences is critical to the development of future clinical candidates. To date, there has been no *in vivo* systematic interrogation of the role of genetic contribution in the ASO-mediated inflammatory response.

The Hybrid Mouse Diversity Panel (HMDP) is a powerful tool for carrying out the investigation of complex traits *in vivo*. It consists of 30 classical inbred mouse strains, in addition to more than 70 recombinant inbred strains, resulting in a panel of more than 100 genetically unique inbred mouse strains. These recombinant inbred strains were derived from intercrosses of eight ''founder strains,'' allowing important insights into genetically derived phenotypic differences among mice. All of the mice in the HMDP are genotyped at 140,000 high-quality single nucleotide polymorphisms (SNPs), with sufficient power to detect traits contributing to 10% of overall phenotypic variance [26–28]. Using the sequenced strains of the HMDP, we can carry out a mouse genome-wide association study (GWAS) to detect SNPs associated with causal variants, contributing to a complex phenotype in a hypothesis-free manner. GWAS generally has been used to identify hundreds of genes contributing to human pathophysiology, including cancer, cardiovascular, metabolic, inflammatory, and neurological diseases [29–32]. Using mouse models in genetic association studies, though not exactly replicating human genetics, provides multiple advantages over human populations, including cost effectiveness, reproducibility of results, and reduced impact of environmental factors.

To better understand the genomic variants that are associated with ASO-mediated inflammation, we employed GWAS and transcriptomic analysis of the HMDP by using an inflammatory ASO (ION 421856) that has previously been shown to induce acute and delayed inflammation *in vivo* [24]. The acute inflammatory response was measured in plasma collected 6 h after a single dose of 75 mg/kg inflammatory or control ASO. Plasma was evaluated for interleukin 6 (IL6), IL10, MCP-1, and MIP-1β production in comparison to mice dosed with a control, noninflammatory ASO in 100 HMDP strains. Delayed response was measured after 96 h by euthanizing the mice and observing increases in spleen weight. We observed significant variability between the HMDP strains for changes in spleen weight and all four markers of acute inflammation, and all markers positively correlated with each other (Supplementary Fig. S1). These results are summarized in Table 1 and Supplementary Table S1. Using Factored Spectrally Transformed Linear Mixed Model (FaST-LMM), we identified a region on chromosome 8 associated with spleen weight increase. Systems genetic analysis suggested this locus contributed to the expression of Rho guanine nucleotide exchange factor 10 (*Arhgef10*). In addition, we identified a locus on chromosome 16 associated with increased MIP-1β plasma levels, and 2 loci on chromosome 17 associated with IL6 and MCP-1 plasma levels. CCAAT/enhancer-binding protein beta (*Cebpb)* was identified as a gene likely to be regulated in *trans* by the region on chromosome 16, whereas both chromosome 17 loci likely regulated salt inducible kinase 1 (*Sik1)*. Additional *in vitro* studies confirmed that *Sik1* contributes to the ASO-mediated acute inflammatory response. Our results demonstrated that genetic variation impacts the *in vivo* inflammatory response to ASOs and validates our use of the HMDP for toxicological evaluation of antisense drugs.

Materials and Methods

Antisense oligonucleotides

2′MOE ASOs were synthesized at Ionis Pharmaceuticals (Carlsbad, CA) as previously described [33]. The

Table 1. Peak Single Nucleotide Polymorphisms Identified by Genome-Wide Association Study for the Indicated Trait in the Hybrid Mouse Diversity Panel Strains After Inflammatory Antisense Oligonucleotide Administration

Trait	*Chromosome*	*Peak SNP*	*Position*	P	*LD block*	*Genes within LD block*
Spleen weight	8	rs13479604	9757872	7.64E-07	9,530,463–11,385,428	7
MIP-1β	16	rs48685261	73451453	2.06E-06	73,258,917–74,084,707	1
IL6	17	rs33060525	35595846	7.80E-07	35,561,965–35,615,192	1
MCP-1	17	rs33441142	34175992	9.69E-07	34,187,385–34,179,669	0

IL, interleukin; LD, linkage disequilibrium; MCP-1, monocyte chemoattractant protein 1; MIP-1β, macrophage inflammatory protein-1β; SNP, single nucleotide polymorphism.

inflammatory ASO (ION 421856) and control (ION 141923) ASOs were formulated in saline and were delivered via subcutaneous injection into the mice.

Mice

An institutional animal care and use committee approved all procedures and protocols for the mouse pharmacology studies. Mice were obtained from The Jackson Laboratory and housed at Ionis Pharmaceuticals, maintained on a chow diet, and entered into studies before they exceeded 7 weeks of age. At 6 h postdose, mice were anesthetized with a controlled flow of isoflurane/oxygen mixture and whole blood ($\sim$100 μL) was collected via orbital bleed with heparinized catheters and EDTA tubes. At 96 h postdose, mice were humanely anesthetized with isoflurane and euthanized by cervical dislocation. Whole blood was immediately collected via cardiac puncture with a 1 cc syringe with a 23G needle. Whole blood was centrifuged in EDTA tubes at 5,000 RPM for 10 min, and plasma was transferred to a 96-well plate and stored −20°C. At necropsy, only spleens and livers were harvested and collected. Spleen and liver samples were separated into several Eppendorf tubes, immediately snap frozen in liquid nitrogen, and stored at −80°C.

Cell lines and reagents

Mouse splenocytes were harvested from naive 7-week-old male C57BL/6 mice, which were anesthetized and euthanized via cervical dislocation. Spleens were pushed through a 0.4 μM cell strainer in 5 mL cold PBS, then slowly pipetted onto 5 mL Lympholyte-M Cell Separation Media (Cedarlane Labs). This mixture was spun at 1,500*g* for 20 min, and the splenocyte layer was harvested and centrifuged at 800*g* for 10 min. The splenocytes were resuspended in RPMI1 supplemented with 10% FBS and 1% penstrep. Live cells were counted by using a TC20 Automated Cell Counter (Biorad) after mixing with Trypsin Blue (Fisher Scientific). Cells were plated at 50,000 cells/well in 96-well round-bottom plates. Inflammatory and control ASOs, lipopolysaccharide (LPS), and HG-9-91-01 were added to the media at the indicated concentrations.

Cytokine/chemokine analysis

Plasma was collected at 6 and 96 h postdose, stored in 96-well plates, and placed at −20°C until use. The main analytes of interest were IL6, IL10, MCP-1, and MIP-1β. MesoScale Discovery developed a custom 4-plex cytokine and chemokine mouse plate. Assay plates were prepared as per the manufacturer's instructions. Twenty-five microliter of plasma per sample was added to 25 μL Meso Scale Discovery (MSD) buffer, and the plates were placed on a shaker plate for 2 h. Each plate was washed three times between each step. Antibody conjugations were prepared per instructions, and the plate was developed and read on a MSD QuickPlex SQ 120. Conjugate levels were normalized to a scale solution on each plate.

RNA analysis

Total mRNA was isolated by using a QIAGEN RNAeasy kit (QIAGEN, Valencia, CA). Target mRNA expression was determined by quantitative polymerase chain reaction (qPCR) using StepOne RT-PCR machines (Applied Biosystems), as previously described. Relative levels of Sik1 were normalized to cyclophilin.

Association analysis

We identified genetic associations by using the FaST-LMM, which is a reformulated mixed-model analysis that performs linearly in run time and memory footprint for GWAS in very large datasets. We retrieved the genotypes from the University of California, Los Angeles (UCLA) systems genetics database along with chromosomal locations of linkage disequilibrium (LD) blocks. The global gene expression microarrays that were generated from microarrays of chow-fed male mice from 95 HMDP strains were obtained from the UCLA systems genetics database. These data were used to perform the *cis* and *trans*-analysis, as previously described. FaST-LMM on ASO accumulation and activity properties was performed with a genome-wide significance threshold of 4.1×10^{-6} as described.

Statistics

Data are reported as means ± S.E.M. The statistical tests and significance are described in the figure legends.

Results

Systems genetics analysis of delayed inflammation-associated SNPs

To identify regions associated with delayed ASO-mediated inflammation, 6-week-old male mice from the HMDP strains were administered one 75 mg/kg dose of either the 2′MOE inflammatory ASO (ION 421856) or the noninflammatory

FIG. 1. Systems genetic analysis identifies *Arhgef10* as a *cis*-eQTL for increased spleen weight after inflammatory ASO administration. **(A)** Six-week-old male mice from 100 HMDP strains ($n = 4$/strain/condition) were dosed with a single 7.5 mg/kg dose of either control ASO (ION 421923) or inflammatory ASO (ION 421856). Spleens were harvested after 96 h, weighed, and recorded as mean percent increase. Results are presented as mean ± S.E.M. (Supplementary Table S1) **(B)** Manhattan plot showing the −log10 of the association *P* values [−log(*P*)] for increased spleen weight in the HMDP strains. Each chromosome is plotted on the *x*-axis in alternating *light* and *dark colors*. Genome-wide significance threshold line is shown in *gray* ($-\log P \leq 5.39$). *Arrow* indicates the location of the significant peak. **(C)** Distribution of percent spleen weight increase based on the genotype of the associated SNP on chromosome 8. Mean ± S.E.M. Two tailed *t*-test, $P \leq 0.0096$ **(D)** Distribution of *Arhgef10* expression by microarray, relative to C57Bl6/J expression, based on the genotype of the associated SNP on chromosome 8. Mean ± S.E.M. Two-tailed *t*-test, $P \leq 0.0024$. **(E)** Percent increase in the spleen weight after inflammatory ASO administration was correlated with *Arhgef10* expression, with the increase significantly lower in strains with high expression by microarray. Mean ± S.E.M. Two-tailed *t*-test, $P \leq 0.0008$. Arhgef10, Rho guanine nucleotide exchange factor 10; ASO, antisense oligonucleotide; eQTL, expression quantitative trait loci; HMDP, hybrid mouse diversity panel; MCP-1, monocyte chemoattractant protein-1; MIP-1β, macrophage inflammatory protein-1β; SNP, single nucleotide polymorphism.

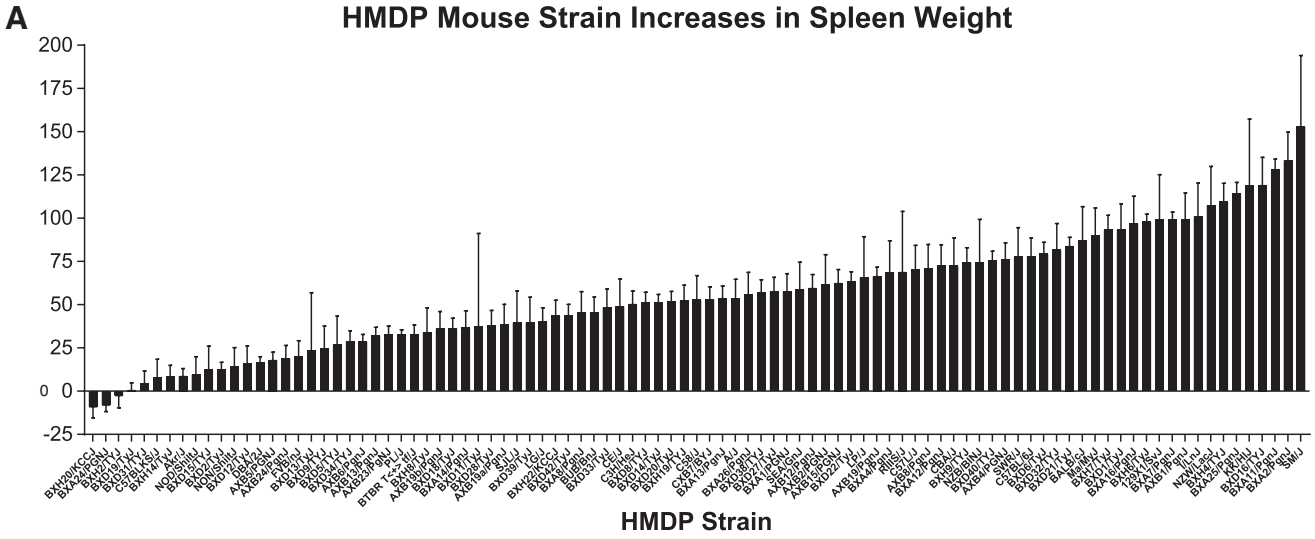
A
HMDP Mouse Strain Increases in Spleen Weight
200
175
150
125
100
75
50
25
0
-25
HMDP Strain

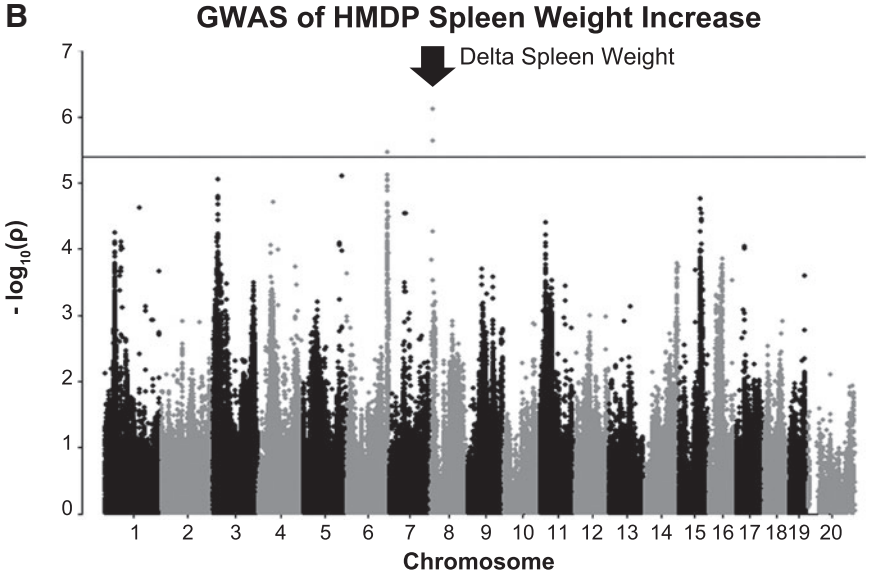
B
GWAS of HMDP Spleen Weight Increase
Delta Spleen Weight
- log10(p)
Chromosome

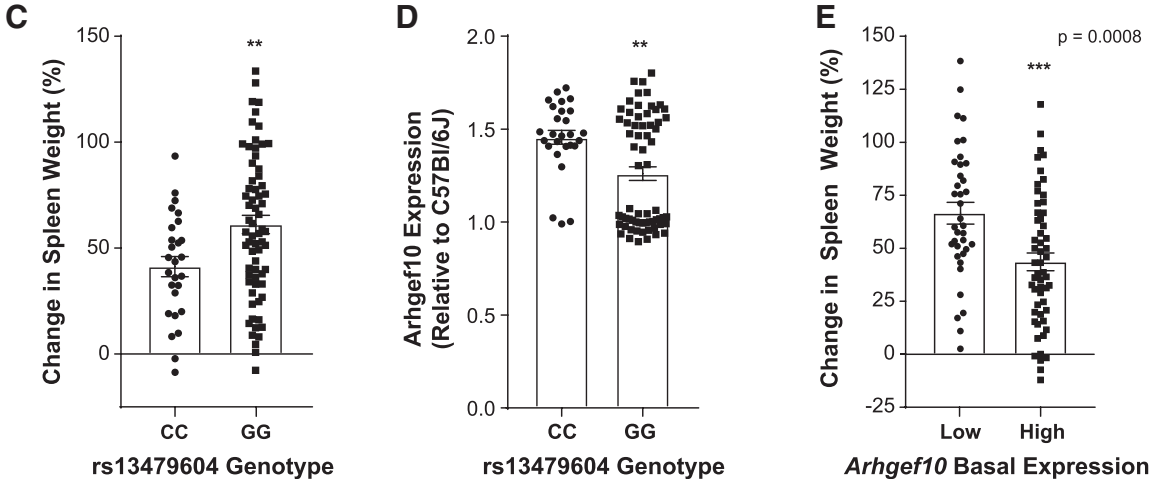
C
Change in Spleen Weight (%)
CC
GG
rs13479604 Genotype
D
Arhgef10 Expression (Relative to C57Bl/6J)
CC
GG
rs13479604 Genotype
E
p = 0.0008
Change in Spleen Weight (%)
Low
High
Arhgef10 Basal Expression

Table 2. Genes Identified as Located Within the Linkage Disequilibrium Block for Peak Single Nucleotide Polymorphism rs13479604, Associated with Increases in Spleen Weight

Gene symbol	*Gene name*	*Localization*
Lig4	Ligase IV, DNA, ATP-dependent	Splenic
Irs2	Insulin receptor substrate 2	Splenic
Col4a1	Collagen, type IV, alpha 1	Splenic
Col4a2	Collagen, type IV, alpha 2	Splenic
Fam155a	Family with sequence similarity 155, member A	Nonsplenic
Myo16	Myosin XVI	Nonsplenic
B930025P03Rik	RIKEN cDNA B930025P03 gene	Nonsplenic

control (ION 141923) ASO (Supplementary Fig. S2). Ninety-six hours after dosing, mice were euthanized and the spleens were removed and weighed (Fig. 1A and Supplementary Table S1).

The association analysis was accomplished via FaST-LMM, where adjusted association *P* values were calculated for 108,064 SNPs with a minor allele frequency of >5% ($P < 0.05$, the genome-wide equivalent for GWA using FaST-LMM in the HMDP is $P \leq 4.1 \times 10^{-6}$, $-\log 10P \leq 5.39$). At this threshold, a genome-wide significant locus associated with variation in increased spleen weight was identified on chromosome 8 (rs13479604, $P \leq 7.63 \times 10^{-7}$) (Fig. 1B, C). This locus contained seven genes within the LD block, four of which are expressed in the spleen (Table 2).

Most SNPs sequenced in the HMDP occur in noncoding regions, making identification of a causal coding mutation unlikely. Therefore, it is important to identify genes within the LD block that also demonstrate expression regulated by the identified SNPs. Isolated macrophages from chow-fed male mice were subjected to global gene expression microarray analysis [34]. These data were used in combination with the SNP data to generate a list of expression quantitative trait loci (eQTL), leading to the identification of *cis*- (within 1 Mb of the peak SNP) and *trans*- (farther than 1 Mb from the peak SNP) regulated genes corresponding to the identified SNP at chromosome 8. *Arhgef10* was found to be regulated in *cis* by this SNP (Supplementary Table S2). This gene has been reported to play a role in inflammation, oxidative stress, thrombus formation, and fibrosis [35]. Further analysis demonstrated that *Arhgef10* expression varied significantly depending on the genotype at SNP rs13479604 (Fig. 1D). Importantly, the basal level of macrophage *Arhgef10* expression across the HMDP was strongly correlated with the increase in spleen weight seen after ASO administration, as mice with higher levels of basal macrophage Arhgef10 expression demonstrated significantly lower increases in spleen weight ($P \leq 0.0008$) (Fig. 1E and Supplementary Fig. S3).

Systems genetics analysis of acute inflammation-associated SNPs

To identify regions associated with acute ASO-mediated inflammation, 6-week-old male mice from the HMDP strains were administered one 75 mg/kg dose of either the 2′MOE inflammatory ASO (ION 421856) or the noninflammatory control (ION 141923) ASO. As previous work has identified peak cytokine production 6 h postdose [24], plasma was isolated and evaluated for IL6, IL10, MCP-1, and MIP-1β concentrations at this time-point (Supplementary Table S1). A wide spectrum in plasma levels for these cytokines was observed. FaST-LMM analysis identified one peak SNP associated with changes in MIP-1β plasma levels in response to ASO administration on chromosome 16 (rs4868521, $P \leq 2.055 \times 10^{-6}$) (Fig. 2B, C). One gene, *Robo2*, was located in the LD block for this locus (Table 1).

As described for the delayed inflammatory phenotype, we performed transcriptomic (eQTL) analysis by using macrophage microarray expression data, accessible on NCBI GEO GSE97207. This effort produced a list of genes that were regulated in *cis* and *trans* by the peak region on chromosome 16. Systems genetics analysis utilizing the macrophage microarray expression data identified 3 genes potentially regulated in *cis* by this peak, and 13 regulated in *trans* (Supplementary Tables S2 and S3). Unusually none of the genes identified in *cis* was found to correlate with the MIP-1β response phenotype. However, macrophage expression *Cebpb*, regulated in *trans*, was found to correlate with the increase in MIP-1β production after administration of the inflammatory ASO (Fig. 2D). Its inclusion in this screen is not surprising as *Cebpb* is a transcription factor expressed in macrophages and has long been known to be responsible for the expression of pro-inflammatory response genes [36].

The IL6 and MCP-1 plasma responses to the inflammatory ASO most closely overlapped out of all the measured endpoints in this study (Supplementary Fig. S1). FaST-LMM analysis of both IL6 and MCP-1 responses identified overlapping peaks on chromosome 17 (Fig. 3), although each had a separate peak SNP (rs33060525, $P \leq 7.8 \times 10^{-7}$ and rs33441142, $P \leq 9.69 \times 10^{-7}$) (Figs. 3D, E, and 4A, B). The rs33060525 locus contained one gene in the LD block, 2300002M23Rik, which has a putative function in extracellular matrix. The rs33441142 loci contained no coding regions within the LD block (Table 1). eQTL analysis performed on these peak SNPs utilizing the macrophage expression microarray data determined that *Sik1* was strongly regulated in *cis* by both SNPs identified in chromosome 17 (Fig. 4C, D and Supplementary Tables S4–S9). Importantly, the peak SNP genotypes strongly correlate with the level of basal macrophage *Sik1* expression. Further, basal *Sik1* expression is significantly negatively correlated with the level of increase seen in plasma IL6 and MCP-1 (Fig. 4E, F).

Validation of Sik1's *role in ASO-associated acute inflammation*

Since *Sik1* plays a key role in the acute inflammatory response, we investigated its putative role in ASO-associated cytokine and chemokine release. Systems analysis of the

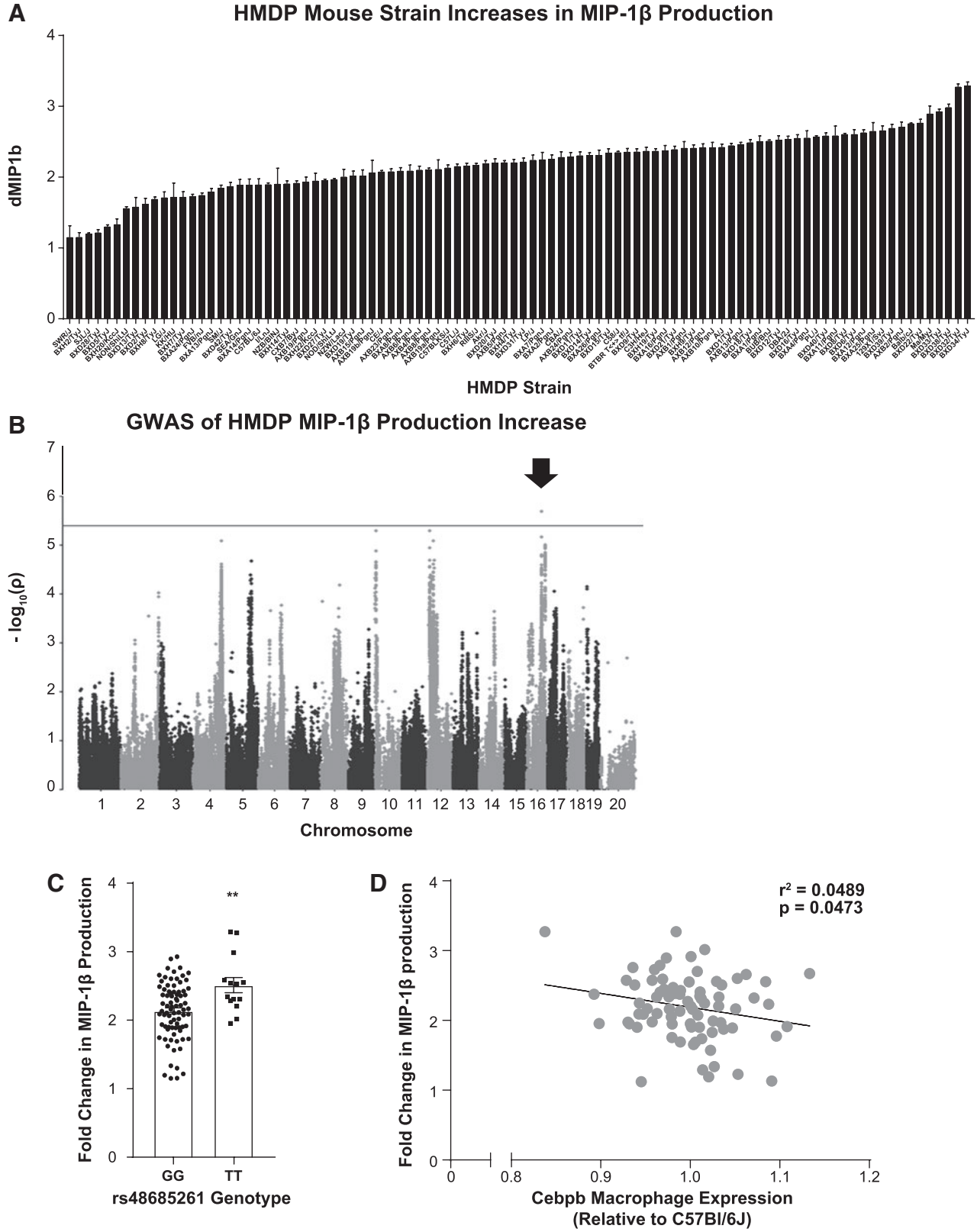

FIG. 2. Systems genetic analysis identifies *Cebpb* as a *trans*-eQTL for MIP-1β production after inflammatory ASO administration. **(A)** Plasma MIP-1β after control and inflammatory ASO exposure are presented as mean fold increase+S.E.M. for all strains tested (Supplementary Table S1). **(B)** Manhattan plot showing the −log(10) of the association *P* values [−log(*P*)] for fold increase in MIP-1β expression in the HMDP strains. Each chromosome is plotted on the *x*-axis in alternating *light* and *dark colors*. Genome-wide significance threshold is shown in *gray* [−log(*P*) = 5.39]. *Arrow* indicates the location of the significant peak. **(C)** Distribution of the fold change in MIP-1β production based on the genotype of the associated SNP on chromosome 16. Mean ± S.E.M. Two tailed *t*-test, $P \leq 0.0021$. **(D)** Fold change in MIP-1β production after inflammatory ASO administration was correlated with *Cebpb* expression measured by microarray relative to C57Bl6J. Linear regression, $P \leq 0.0473$. Cebpb, CCAAT/enhancer-binding protein beta.

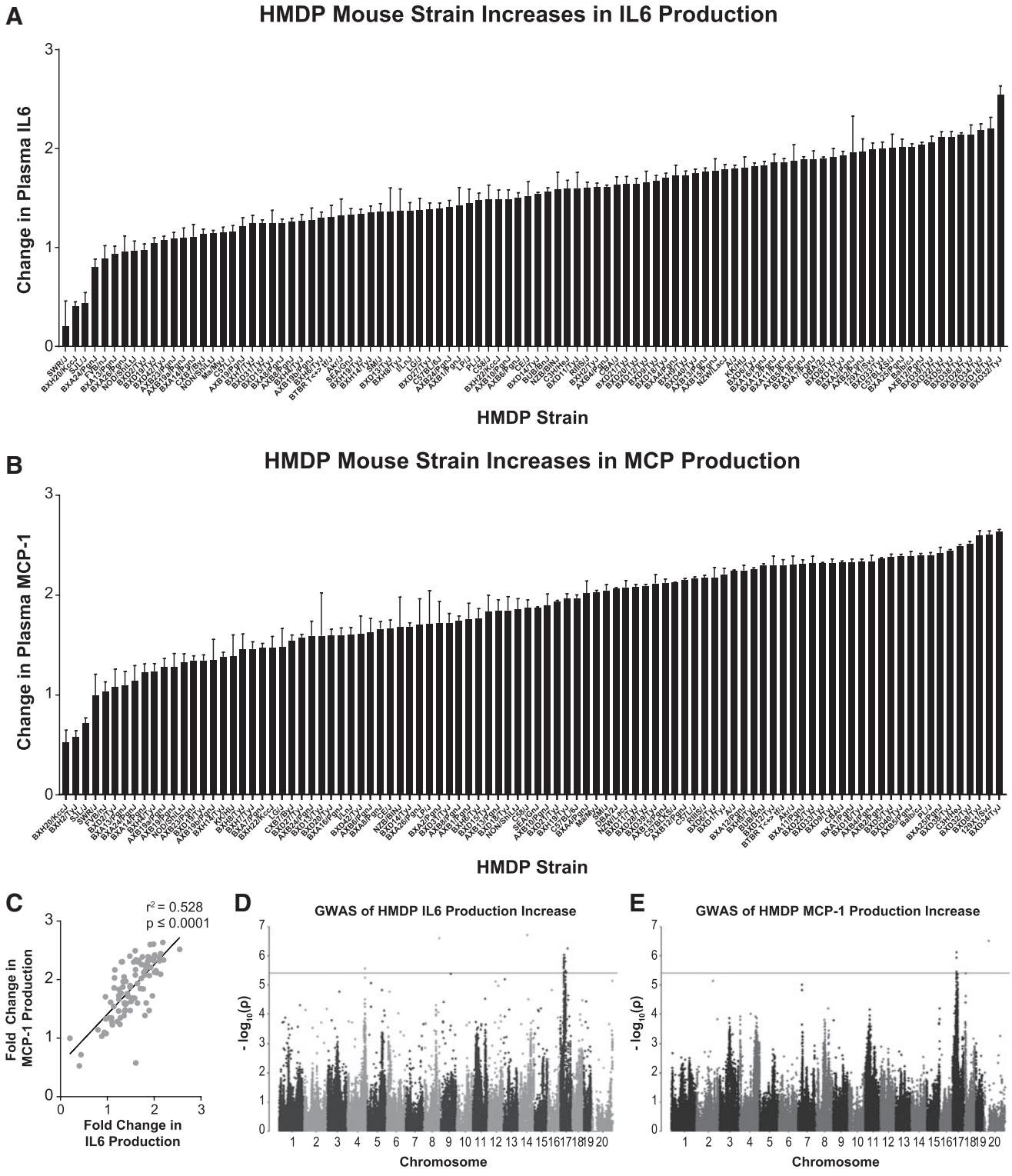

FIG. 3. IL6 and MCP-1 production after inflammatory ASO administration are closely correlated. **(A)**. Plasma IL6 after control and inflammatory ASO exposure are presented as mean fold increase+S.E.M. for all strains tested (Supplementary Table S1). **(B)** As with IL6, plasma was analyzed by MSD plate ELISA for MCP-1 production and recorded as fold increase (Supplementary Table S1). **(C)** IL6 and MCP-1-fold increase were the most closely correlated endpoints out of all inflammatory endpoints in this study. Linear regression, $P < 0.0001$. **(D)** Manhattan plot showing the −log(10) of the association P values [−log(P)] for fold increase in IL6 expression in the HMDP strains. Each chromosome is plotted on the x-axis in alternating *light* and *dark colors*. Genome-wide significance threshold is shown in *gray* [−log(P) = 5.39]. *Arrow* indicates the location of the significant peak. **(E)** As with IL6, Manhattan plot for MCP-1 production following the same parameters. IL, interleukin; MSD, Meso Scale Discovery.

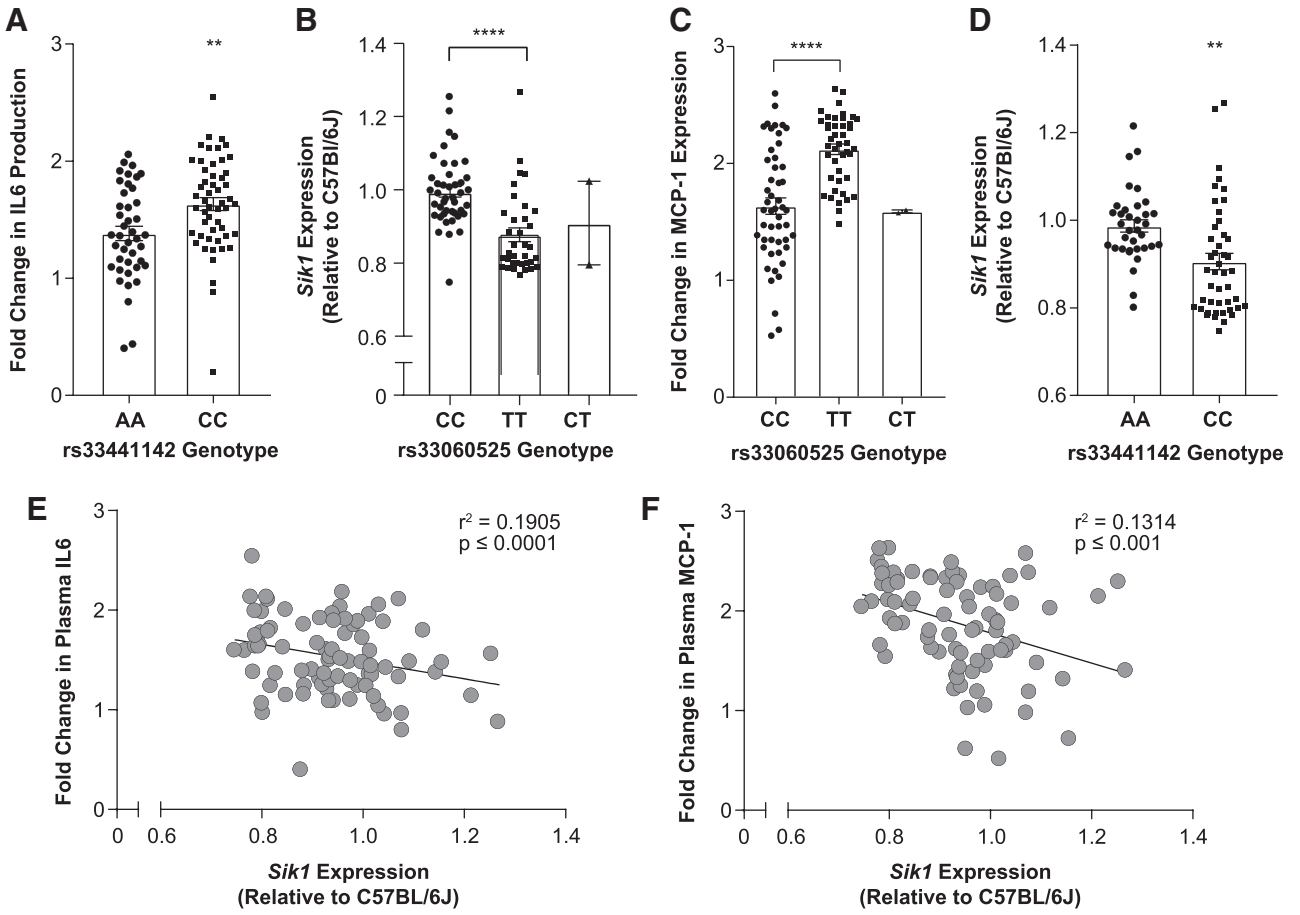

FIG. 4. Systems genetic analysis identifies *Sik1* as a *cis*-eQTL for IL6 and MCP-1 production after inflammatory ASO administration. **(A)** Distribution of the fold change in IL6 production based on the genotype of the associated SNP on chromosome 17. Mean ± S.E.M. Two-tailed *t*-test, $P \leq 0.0016$. **(B)** Distribution of *Sik1* expression by microarray relative to C57Bl/6J expression based on the genotype of the associated SNP on chromosome 17. Mean ± S.E.M. Two-tailed *t*-test, $P \leq 0.0032$. **(C)** Distribution of the fold change in MCP-1 production based on the genotype of the associated SNP on chromosome 17. Mean ± S.E.M. Two-tailed *t*-test, $P < 0.0001$. **(D)** Distribution of *Sik1* expression by microarray relative to C57Bl/6J based on the genotype of the associated SNP on chromosome 17. Mean ± S.E.M. Two-tailed *t*-test, $P < 0.0001$. **(E)** Fold change in IL6 production after inflammatory ASO administration was correlated with *Sik1* expression measured by microarray relative to C57Bl/6J. Linear regression, $P < 0.0001$. **(F)** Fold change in MCP-1 production after inflammatory ASO administration was correlated with *Sik1* expression measured by microarray relative to C57Bl/6J. Linear regression, $P \leq 0.0009$. Sik1, salt inducible kinase 1.

peak SNPs rs33060525 and rs33441142 demonstrated a significant difference in plasma MCP-1 and MIP-1β levels based on the genotype distribution at those SNPs. Further, our analysis determined that HMDP strains with lower *Sik1* expression had significantly higher IL6 and MCP-1 plasma levels after ASO administration.

To experimentally validate the role of *Sik1*, we utilized the pan-SIK inhibitor HG-9-91-01 in mouse primary splenocytes isolated from healthy C57Bl6/J mice [37]. These splenocytes were pretreated with HG-9-91-01 for 3 h and subsequently exposed to either a control ASO, an inflammatory ASO, or LPS for 24 h. MSD analysis of the cell culture media demonstrated that splenocytes treated with HG-9-91-01 displayed a significantly increased release of MCP-1 and IL6, but not IL10 or MIP-1β (Fig. 5). Further, this correlation between *Sik1* inhibition and increased IL6 and MCP-1 release was seen across multiple strains of mice, validating *Sik1* as an important mediator of ASO-associated acute inflammation (Supplementary Fig. S4).

Discussion

Innovations in medicinal chemistry have drastically improved ASO activity and target tissue specificity, allowing increasingly lower doses of drug to be administered in the clinic. Although antisense therapeutics are well tolerated in the clinic, ongoing research efforts seek to identify factors that allow some sequences to induce a proinflammatory response in the murine models. Although these problematic sequences are quickly identified and removed well before reaching the clinic, more efforts are needed to better understand the mechanism of this response.

Here, we investigate the role of genetics in modulating the response to an inflammatory ASO sequence *in vivo*. Our data

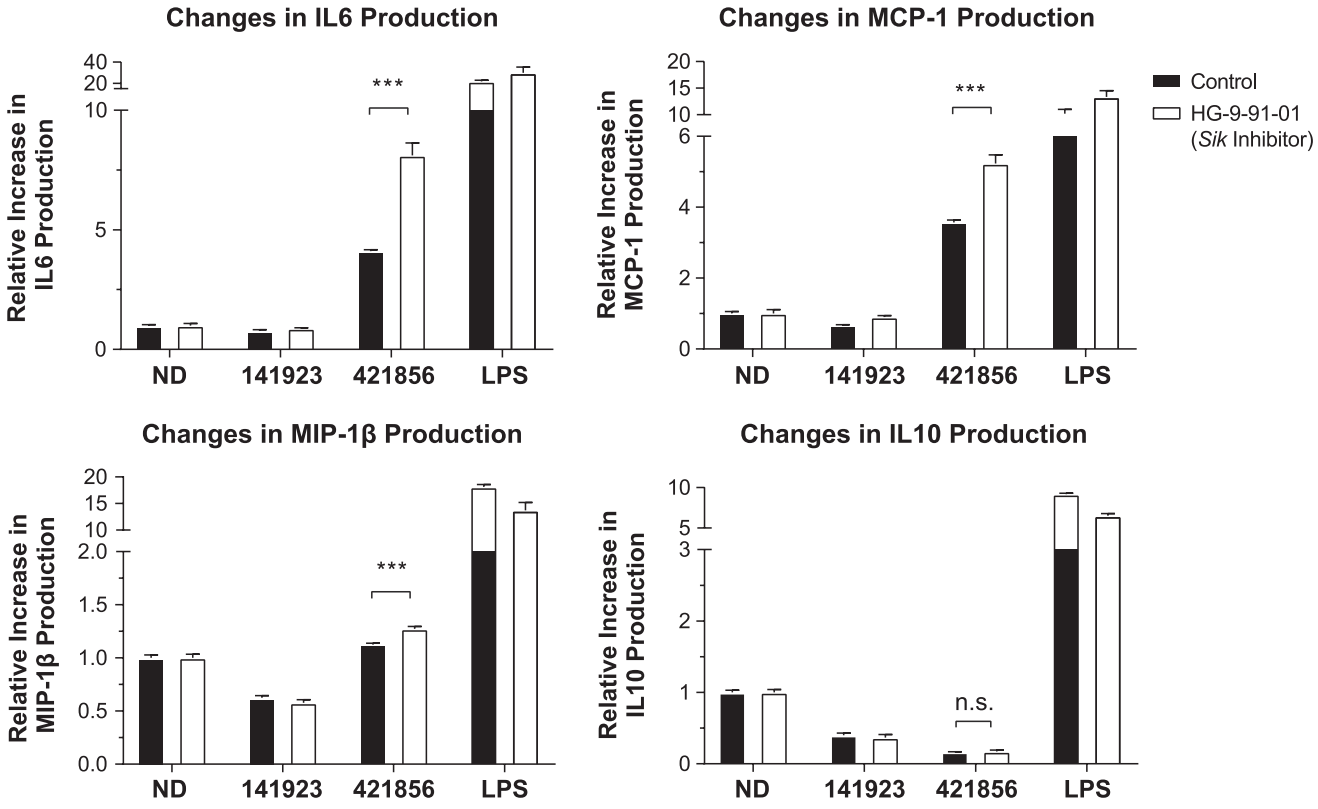

FIG. 5. Validation of the role of *Sik1* in acute inflammation in response to inflammatory ASO administration. Splenocytes were harvested from 7-week-old male mice as described. They were pretreated with either HG-9-91-01 or DMSO for 3 h; then, they were treated with either control ASO (ION 421923), an inflammatory ASO (ION 421856). or 4 μg LPS. Significant increases in production of IL6, MCP-1, and MIP-1β were observed in response to the inflammatory ASO when pretreated with the SIK inhibitor. LPS, lipopolysaccharide.

show that, after a single dose of a proinflammatory 2′MOE ASO, the plasma levels of IL6, IL10, MCP-1, and MIP-1β vary significantly among the 100 genetically unique HMDP strains. In a delayed response, spleen weights also vary significantly between the mice. The variability in these parameters allowed us to perform GWAS and led to the identification of inflammatory ASO-associated eQTLs *Arhgef10*, associated with increased spleen weight, *Cebpb*, associated with increased MIP-1β, and *Sik1*, associated with production of IL6 and MCP-1. No significant peaks were seen in the GWAS for IL10 production (Supplementary Fig. S5). These results are particularly noteworthy as *Cebpb* and *Sik1* are known to be involved with TLR signaling, which has been previously shown to be crucial for the acute ASO-mediated inflammatory process.

Systems genetics analysis identified *Cepbp* as a *trans*-eQTL, concordant with the peak SNP identified in GWAS analysis of MIP-1β increase. Further analysis showed that its expression correlated with MIP-1β plasma levels after inflammatory ASO administration. *Cebpb*, a member of the CCAAT/enhancer-binding protein family, is a transcription factor strongly regulated by the TLRs and NF-κB pathway and is known to mediate the expression of a variety of inflammatory factors, including MIP-1β [36,38]. The gene encoding MIP-1β protein contains a *Cebpb* regulatory motif in the promoter [39]. The identification of *Cebpb* is not surprising in a study examining factors involved in inflammation and its inclusion serves as an important control validating the use of the HMDP.

Systems genetics analysis identified *Sik1* as a gene with expression concordant with the identified SNPs rs33060525 and rs33441142. Further analysis showed that increasing levels of *Sik1* expression among the HMDP mice led to decreased production of IL6 and MCP-1 in plasma after inflammatory ASO administration. The genetic data were further confirmed *in vivo* by the use of the SIK inhibitor HG-9-91-01 in mouse primary splenocytes, which showed increased IL6 and MCP-1 production when treated with an inflammatory ASO in conjunction with the SIK inhibitor.

Sik1 is a member of a family of related serine-threonine kinases that have been implicated in controlling liver glucose homeostasis, hepatic lipogenesis, steroidogenesis, adipogenesis, and TLR-mediated inflammation [40–43]. Canonically, the SIKs control the phosphorylation and subcellular localization of class IIa histone deacetylases (HDACs) and cAMP-regulated transcriptional coactivators (CRTCs) [44,45]. Notably, *Sik1* expression has been found to inhibit NF-κB activation in response to TLR signaling, resulting in decreased expression and production of proinflammatory cytokines both *in vitro* and *in vivo* [43,46], and Sik3 has been shown to negatively regulate the production of IL6, nitric oxide, and IL12p40 *in vivo* [47]. Our data are in line with these published reports, confirming the role of *Sik1* as a mediator of ASO-induced NF-κB activation.

Arhgef10 was identified as a *cis*-eQTL regulated by a peak SNP strongly associated with increases in spleen weight. Systems genetics analysis of this gene showed that its

expression was further correlated with the delayed inflammatory phenotype. SNPs in *Arhgef10* have been linked with the incidence of thrombotic stroke in humans; however, the function of this gene is not well understood [35]. It is a member of the family of guanidine nucleotide exchange factors, which catalyze the exchange of bound GDP by GTP, thereby regulating the activity of small Rho-GTPases [48]. The best-known function of *Arhgef10* is to regulate the activity of RhoA kinase (ROCK); *Arhgef10* upregulation has been found to increase the activity of ROCK *in vivo* [35]. Importantly, *Rock2* has been found by our group to be involved in the activity of ASOs *in vivo*, suggesting that *Arhgef10* is a possible link between ASO activity and inflammation [49]. Further, the RhoA-Rho kinase pathway has been shown to regulate a wide variety of functions, including endothelial dysfunction, inflammation, and apoptosis, and can be induced by LPS exposure [50–52]. Specifically, it has been demonstrated that *ROCK1* negatively regulates splenic erythropoiesis via regulation of *P53*, important in the development of the delayed inflammatory phenotype in response to ASO [53].

Surprisingly, although TLR9 is a complex pathway, other intermediaries of its downstream activation were not identified. Closer analysis of HMDP macrophage expression found that TLR9, similar to many, though expressed, did not sufficiently vary in its expression across the HMDP strains (Supplementary Fig. S6), making identification using the HMDP unlikely.

In summary, genetic factors have been shown for the first time to be capable of altering the ASO-mediated inflammatory response *in vivo*. Here, we establish the utility of the HMDP as a method for detecting genes modulating the inflammatory response to ASOs in an *in vivo* setting. Future work will focus on translating these findings to human systems and applying this understanding to more efficiently screen ASOs preclinically. Further studies evaluating these factors will provide us with a better understanding of ASO response, potential effects across patient populations and help design drugs with improved therapeutic benefits.

Acknowledgments

Ionis Pharmaceuticals, Inc. approved and sponsored the study design, data collection, analysis, and preparation of this article. Supported authors E.P., P.C., W.F., S.R., J.H., S.A.B., P.N., R.M.C., and R.G.L. The National Institute of Health sponsored data collection. HL28481, HL30568, HL114437, and HL123295 supported authors C.P. and A.J.L. The authors would like to thank the vivarium staff, preclinical toxicity group (Todd Machemer), bioinformatics group, the members of the cardiovascular research group (Amy Wei, Steve Yeh, PhD, Adam Mullick, PhD, Stan Riney), and Tracey Riegle who have provided crucial help with animal housing, experimental techniques, and discussions during preparation of this article.

Declarations

Ethics Statement

Ionis is AAALAC accredited and follows the 8th Ed. Of the Guide for the Care and Use of Laboratory Animals and the 2013 AVMA guidelines for the euthanasia of animals. All animals in this study were anesthetized with Isoflurane and euthanized via cervical dislocation. The Ionis IACUC-approved protocol is No. P-0225. This protocol was approved on May 28, 2014.

Availability of data and material

All macrophage microarray expression data are available at NCBI GEO GSE97207 (www.ncbi.nlm.nih.gov/geo/query/acc.cgi?acc=GSE97207).

Author Disclosure Statement

E.P., P.C., W.F., S.R., J.H., S.A.B., P.N., R.M.C., and R.G.L. were employees at Ionis Pharmaceuticals when these studies were completed.

Supplementary Material

Supplementary Figure S1
Supplementary Figure S2
Supplementary Figure S3
Supplementary Figure S4
Supplementary Figure S5
Supplementary Figure S6
Supplementary Table S1
Supplementary Table S2
Supplementary Table S3
Supplementary Table S4
Supplementary Table S5
Supplementary Table S6
Supplementary Table S7
Supplementary Table S8
Supplementary Table S9

References

1. Raal FJ, RD Santos, DJ Blom, AD Marais, MJ Charng, WC Cromwell, RH Lachmann, D Gaudet, JL Tan, *et al*. (2010). Mipomersen, an apolipoprotein B synthesis inhibitor, for lowering of LDL cholesterol concentrations in patients with homozygous familial hypercholesterolaemia: a randomised, double-blind, placebo-controlled trial. Lancet 375:998–1006.
2. Jaschinski F, T Rothhammer, P Jachimczak, C Seitz, A Schneider and KH Schlingensiepen. (2011). The antisense oligonucleotide trabedersen (AP 12009) for the targeted inhibition of TGF-beta2. Curr Pharm Biotechnol 12:2203–2213.
3. Al-Asaaed S and E Winquist. (2013). Custirsen (OGX-011): clusterin inhibitor in metastatic prostate cancer. Curr Oncol Rep 15:113–118.
4. Janssen HL, HW Reesink, EJ Lawitz, S Zeuzem, M Rodriguez-Torres, K Patel, AJ van der Meer, AK Patick, A Chen, *et al*. (2013). Treatment of HCV infection by targeting microRNA. N Engl J Med 368:1685–1694.
5. Jones NR, MA Pegues, MA McCrory, W Singleton, C Bethune, BF Baker, DA Norris, RM Crooke, MJ Graham and AJ Szalai. (2012). A selective inhibitor of human C-reactive protein translation is efficacious in vitro and in C-reactive protein transgenic mice and humans. Mol Ther Nucleic Acids 1:e52.
6. Hua Y, K Sahashi, F Rigo, G Hung, G Horev, CF Bennett and AR Krainer. (2011). Peripheral SMN restoration is

essential for long-term rescue of a severe spinal muscular atrophy mouse model. Nature 478:123–126.
7. Kordasiewicz HB, LM Stanek, EV Wancewicz, C Mazur, MM McAlonis, KA Pytel, JW Artates, A Weiss, SH Cheng, *et al*. (2012). Sustained therapeutic reversal of huntington's disease by transient repression of huntingtin synthesis. Neuron 74:1031–1044.
8. Crooke ST. (2004). Antisense strategies. Curr Mol Med 4: 465–487.
9. Lee RG, J Crosby, BF Baker, MJ Graham and RM Crooke. (2013). Antisense technology: an emerging platform for cardiovascular disease therapeutics. J Cardiovasc Transl Res 6:969–980.
10. Krieg AM. (1996). An innate immune defense mechanism based on the recognition of CpG motifs in microbial DNA. J Lab Clin Med 128:128–133.
11. Monteith DK, SP Henry, RB Howard, S Flournoy, AA Levin, CF Bennett and ST Crooke. (1997). Immune stimulation—a class effect of phosphorothioate oligodeoxynucleotides in rodents. Anticancer Drug Des 12:421–432.
12. Roberts TL, MJ Sweet, DA Hume and KJ Stacey. (2005). Cutting edge: species-specific TLR9-mediated recognition of CpG and non-CpG phosphorothioate-modified oligonucleotides. J Immunol 174:605–608.
13. Burel SA, T Machemer, FL Ragone, H Kato, P Cauntay, S Greenlee, A Salim, WA Gaarde, G Hung, *et al*. (2012). Unique O-methoxyethyl ribose-DNA chimeric oligonucleotide induces an atypical melanoma differentiation-associated gene 5-dependent induction of type I interferon response. J Pharmacol Exp Ther 342:150–162.
14. Henry S, K Stecker, D Brooks, D Monteith, B Conklin and CF Bennett. (2000). Chemically modified oligonucleotides exhibit decreased immune stimulation in mice. J Pharmacol Exp Ther 292:468–479.
15. Younis HS, T Vickers, AA Levin and SP Henry. (2006). CpG and non-CpG oligodeoxynucleotides induce differential proinflammatory gene expression profiles in liver and peripheral blood leukocytes in mice. J Immunotoxicol 3: 57–68.
16. Akira S and H Hemmi. (2003). Recognition of pathogen-associated molecular patterns by TLR family. Immunol Lett 85:85–95.
17. Akira S and K Takeda. (2004). Toll-like receptor signalling. Nat Rev Immunol 4:499–511.
18. Kawai T and S Akira. (2010). The role of pattern-recognition receptors in innate immunity: update on toll-like receptors. Nat Immunol 11:373–384.
19. Kawai T and S Akira. (2011). Toll-like receptors and their crosstalk with other innate receptors in infection and immunity. Immunity 34:637–650.
20. Krieg AM, AK Yi, S Matson, TJ Waldschmidt, GA Bishop, R Teasdale, GA Koretzky and DM Klinman. (1995). CpG motifs in bacterial DNA trigger direct B-cell activation. Nature 374:546–549.
21. Bauer S, CJ Kirschning, H Hacker, V Redecke, S Hausmann, S Akira, H Wagner and GB Lipford. (2001). Human TLR9 confers responsiveness to bacterial DNA via species-specific CpG motif recognition. Proc Natl Acad Sci U S A 98:9237–9242.
22. Blasius AL and B Beutler. (2010). Intracellular toll-like receptors. Immunity 32:305–315.
23. Sirois CM, T Jin, AL Miller, D Bertheloot, H Nakamura, GL Horvath, A Mian, J Jiang, J Schrum, *et al*. (2013). Rage is a nucleic acid receptor that promotes inflammatory responses to DNA. J Exp Med 210:2447–2463.
24. Paz S, J Hsiao, P Cauntay, A Soriano, L Bai, T Machemer, X Xiao, S Guo, G Hung, *et al*. (2017). The distinct and cooperative roles of toll-like receptor 9 and receptor for advanced glycation end products in modulating in vivo inflammatory responses to select CpG and non-CpG oligonucleotides. Nucleic Acid Ther 27:272–284.
25. Senn JJ, S Burel and SP Henry. (2005). Non-CpG-containing antisense 2′-methoxyethyl oligonucleotides activate a proinflammatory response independent of toll-like receptor 9 or myeloid differentiation factor 88. J Pharmacol Exp Ther 314:972–979.
26. Ghazalpour A, CD Rau, CR Farber, BJ Bennett, LD Orozco, A van Nas, C Pan, H Allayee, SW Beaven, *et al*. (2012). Hybrid mouse diversity panel: a panel of inbred mouse strains suitable for analysis of complex genetic traits. Mamm Genome 23:680–692.
27. Bennett BJ, CR Farber, L Orozco, HM Kang, A Ghazalpour, N Siemers, M Neubauer, I Neuhaus, R Yordanova, *et al*. (2010). A high-resolution association mapping panel for the dissection of complex traits in mice. Genome Res 20:281–290.
28. Rau CD, B Parks, Y Wang, E Eskin, P Simecek, GA Churchill and AJ Lusis. (2015). High-density genotypes of inbred mouse strains: improved power and precision of association mapping. G3 (Bethesda) 5:2021–2026.
29. Hui ST, BW Parks, E Org, F Norheim, N Che, C Pan, LW Castellani, S Charugundla, DL Dirks, *et al*. (2015). The genetic architecture of NAFLD among inbred strains of mice. Elife 4:e05607.
30. Farber CR, BJ Bennett, L Orozco, W Zou, A Lira, E Kostem, HM Kang, N Furlotte, A Berberyan, *et al*. (2011). Mouse genome-wide association and systems genetics identify Asxl2 as a regulator of bone mineral density and osteoclastogenesis. PLoS Genet 7:e1002038.
31. Parks BW, T Sallam, M Mehrabian, N Psychogios, ST Hui, F Norheim, LW Castellani, CD Rau, C Pan, *et al*. (2015). Genetic architecture of insulin resistance in the mouse. Cell Metab 21:334–346.
32. Rau CD, J Wang, R Avetisyan, MC Romay, L Martin, S Ren, Y Wang, and Lusis. (2015). Mapping genetic contributions to cardiac pathology induced by beta-adrenergic stimulation in mice. Circ Cardiovasc Genet 8:40–49.
33. Watts LM, VP Manchem, TA Leedom, AL Rivard, RA McKay, D Bao, T Neroladakis, BP Monia, DM Bodenmiller, *et al*. (2005). Reduction of hepatic and adipose tissue glucocorticoid receptor expression with antisense oligonucleotides improves hyperglycemia and hyperlipidemia in diabetic rodents without causing systemic glucocorticoid antagonism. Diabetes 54:1846–1853.
34. Sallam T, M Jones, BJ Thomas, X Wu, T Gilliland, K Qian, A Eskin, D Casero, Z Zhang, *et al*. (2018). Transcriptional regulation of macrophage cholesterol efflux and atherogenesis by a long noncoding RNA. Nat Med 24:304–312.
35. Matsushita T, K Ashikawa, K Yonemoto, Y Hirakawa, J Hata, H Amitani, Y Doi, T Ninomiya, T Kitazono, *et al*. (2010). Functional SNP of ARHGEF10 confers risk of atherothrombotic stroke. Hum Mol Genet 19:1137–1146.
36. Tsukada J, Y Yoshida, Y Kominato and PE Auron. (2011). The CCAAT/enhancer (C/EBP) family of basic-leucine zipper (bZIP) transcription factors is a multifaceted highly-regulated system for gene regulation. Cytokine 54:6–19.

37. Sundberg TB, HG Choi, JH Song, CN Russell, MM Hussain, DB Graham, B Khor, J Gagnon, DJ O'Connell, *et al*. (2014). Small-molecule screening identifies inhibition of salt-inducible kinases as a therapeutic strategy to enhance immunoregulatory functions of dendritic cells. Proc Natl Acad Sci U S A 111:12468–12473.
38. Hirata M, F Kugimiya, A Fukai, S Ohba, N Kawamura, T Ogasawara, Y Kawasaki, T Saito, F Yano, *et al*. (2009). C/EBPbeta promotes transition from proliferation to hypertrophic differentiation of chondrocytes through transactivation of p57. PLoS One 4:e4543.
39. Zhang Z, JL Bryan, E DeLassus, LW Chang, W Liao and LJ Sandell. (2010). CCAAT/enhancer-binding protein β and NF-κB mediate high level expression of chemokine genes CCL3 and CCL4 by human chondrocytes in response to IL-1β. J Biol Chem 285:33092–33103.
40. Qu C and Y Qu. (2017). Down-regulation of salt-inducible kinase 1 (SIK1) is mediated by RNF2 in hepatocarcinogenesis. Oncotarget 8:3144–3155.
41. Yoon YS, WY Seo, MW Lee, ST Kim and SH Koo. (2009). Salt-inducible kinase regulates hepatic lipogenesis by controlling SREBP-1c phosphorylation. J Biol Chem 284: 10446–10452.
42. Nixon M, R Stewart-Fitzgibbon, J Fu, D Akhmedov, K Rajendran, MG Mendoza-Rodriguez, YA Rivera-Molina, M Gibson, ED Berglund, NJ Justice and R Berdeaux. (2016). Skeletal muscle salt inducible kinase 1 promotes insulin resistance in obesity. Mol Metab 5:34–46.
43. Yong Kim S, S Jeong, KH Chah, E Jung, KH Baek, ST Kim, JH Shim, E Chun and KY Lee. (2013). Salt-inducible kinases 1 and 3 negatively regulate toll-like receptor 4-mediated signal. Mol Endocrinol 27:1958–1968.
44. Wein MN, M Foretz, DE Fisher, RJ Xavier and HM Kronenberg. (2018). Salt-inducible kinases: physiology, regulation by camp, and therapeutic potential. Trends Endocrinol Metab 29:723–735.
45. Clark K, KF MacKenzie, K Petkevicius, Y Kristariyanto, J Zhang, HG Choi, M Peggie, L Plater, PG Pedrioli, *et al*. (2012). Phosphorylation of CRTC3 by the salt-inducible kinases controls the interconversion of classically activated and regulatory macrophages. Proc Natl Acad Sci U S A 109:16986–16991.
46. Zhang Y, W Gao, K Yang, H Tao and H Yang. (2018). Salt-inducible kinase 1 (SIK1) is induced by alcohol and suppresses microglia inflammation via NF-κB signaling. Cell Physiol Biochem 47:1411–1421.
47. Sanosaka M, M Fujimoto, T Ohkawara, T Nagatake, Y Itoh, M Kagawa, A Kumagai, H Fuchino, J Kunisawa, T Naka and H Takemori. (2015). Salt-inducible kinase 3 deficiency exacerbates lipopolysaccharide-induced endotoxin shock accompanied by increased levels of pro-inflammatory molecules in mice. Immunology 145:268–278.
48. Rossman KL, CJ Der and J Sondek. (2005). GEF means go: turning on RHO GTPases with guanine nucleotide-exchange factors. Nat Rev Mol Cell Biol 6:167–180.
49. Pirie E, S Ray, C Pan, W Fu, AF Powers, D Polikoff, CM Miller, KM Kudrna, EN Harris, *et al*. (2018). Mouse genome-wide association studies and systems genetics uncover the genetic architecture associated with hepatic pharmacokinetic and pharmacodynamic properties of a constrained ethyl antisense oligonucleotide targeting malat1. PLoS Genet 14:e1007732.
50. Loirand G, E Scalbert, A Bril and P Pacaud. (2008). Rho exchange factors in the cardiovascular system. Curr Opin Pharmacol 8:174–180.
51. Mong PY and Q Wang. (2009). Activation of Rho kinase isoforms in lung endothelial cells during inflammation. J Immunol 182:2385–2394.
52. Wang C, S Song, Y Zhang, Y Ge, X Fang, T Huang, J Du and J Gao. (2015). Inhibition of the Rho/Rho kinase pathway prevents lipopolysaccharide-induced hyperalgesia and the release of TNF-alpha and IL-1beta in the mouse spinal cord. Sci Rep 5:14553.
53. Vemula S, J Shi, RS Mali, P Ma, Y Liu, P Hanneman, KR Koehler, E Hashino, L Wei and R Kapur. (2012). Rock1 functions as a critical regulator of stress erythropoiesis and survival by regulating p53. Blood 120:2868–2878.

Address correspondence to:
Richard G. Lee, PhD
Ionis Pharmaceuticals
2855 Gazelle Court
Carlsbad, CA 92008

E-mail: rlee@ionisph.com

Received for publication April 10, 2019; accepted after revision June 4, 2019.